Meso FE simulation of composite reinforcement deformation based on X-ray computed tomography

Naïm Naouar, Emmanuelle Vidal-Sallé, Philippe Boisse

Meso F.E. Simulation of Composite Reinforcement Deformation based on X-ray Computed Tomography

Naim NAOUAR[1,a)], Emmanuelle VIDAL-SALLE[1] and Philippe BOISSE[1]

[1] *Univ Lyon, INSA-Lyon, CNRS UMR5259, LaMCoS, F-69621, France*

[a)] Corresponding author: naim.naouar@insa-lyon.fr

Abstract. Meso-FE modelling of 3D textile composites is a powerful tool, which can help determine mechanical properties and permeability of the reinforcements or composites. The quality of the meso FE analyses depends on the quality of the initial model. A direct method based on X-ray tomography imaging is introduced to determine finite element models based on the real geometry of 3D composite reinforcements. The method is particularly suitable regarding 3D textile reinforcements for which internal geometries are numerous and complex. An analysis of the image's texture is performed. A hyperelastic model developed for fibre bundles is used for the simulation of the deformation of the 3D reinforcement.

INTRODUCTION

The present paper aims to perform 3D F.E. analyses of the 3D reinforcement based on a model obtained from X-ray tomography in order to be as close as possible of the real geometry of the 3D reinforcement. The quality of a meso FE analysis strongly depends on the F.E. model, its geometry and the associated data, most important of which being the fibre directions. The geometry can be obtained with textile geometrical simulators such as TexGen or WiseTex [1,2]. Nevertheless, they provide an idealized geometry of the reinforcements which cannot take into account the geometrical imperfections or specificities of the material being analysed. Moreover, reinforcement architectures are diversified and complex for 3D fabrics and all the geometrical possibilities cannot be described by these simulators. In some cases, when the textile reinforcement is thick, and complex, the internal geometry is not completely known. Lastly, interpenetration can occur between the yarns defined by the simulators in some configurations. In the present study, the initial geometry of the meso-FE model of a 3D composite reinforcement is directly obtained from X-ray Micro Tomography (XRMT) also called micro computed tomography (μCT) [3]. This fairly recent technique allows for detailed, accurate and non-destructive 3D observations inside a material especially for composites and composite reinforcements [4,5]. It distinguishes yarns and even fibres and defines the anisotropic directions of the material. In the present paper, a methodology is used to build automatically finite element models from X-ray micro CT images of 3D composite reinforcements. These models take into account the specificities of the analysed material's geometry. They can be obtained for any reinforcement's weaving style or architecture. A meso FE modelling of a 3D orthogonal non-crimp woven fabric deformation is taken as an example. A new segmentation method is used. It is based on the analysis of image texture. For 2D fabrics, the separation of the warp and weft yarns can be obtained by using the structural tensor of the fibre's direction [4]. This is not possible for 3D reinforcements because the fibres flow in three-dimensional space. An approach based on texture analysis for images is used for the 3D composite reinforcement. A method is then submitted to build a prismatic mesh of the yarns. Meso F.E. analysis of the 3D RUC's deformation uses a hyperelastic law for finite strains of fibrous yarns [6]. After a compaction, the internal geometry of the computed and of the experimental 3D reinforcement are compared.

SEGMENTATION

A finite element model is built from tomography images. The pictures extracted from the CT need to undergo a segmentation process in order to differentiate the wrap, weft and binder yarns. This phase of the process is critical

because it impacts the quality of the model significantly. Several segmentation methods are available, one of them, based on the images structural tensor, seems interesting [4]. This tensor defines the orientation of fibres in a yarn. This method is efficient if the picture display stringy yarns. It is generally the case for 2D reinforcements. In certain situations, the segmentation based on the orientation tensor cannot be used because the results from the scanning process leads to pictures without stringy yarns but with a grainy aspect. This occurs in 3D reinforcements for images that are perpendicular to or cut the yarns. The present work is based on a Texture Analysis for Image segmentation that is outlined below. This method differentiates 3D reinforcement yarns well.

Grey Level Co-Occurrence Matrix

Texture Analysis for Image Segmentation is based on the calculation of Grey Level Co-occurrence Matrix (GLC Matrix) [7] . This method highlights pixel pairs spatially separated by a translation.

The GLC Matrix calculates how often a pixel with grey-level (greyscale intensity) value i occurs horizontally adjacent to a pixel with the value j. Each element (i, j) in the GLC Matrix specifies the number of times that the pixel with value i occurs horizontally adjacent to a pixel with value j in the input image. Figure 1 shows on the left a matrix that represents an input image of size 4 x 4 and contains five grey levels (0-4).

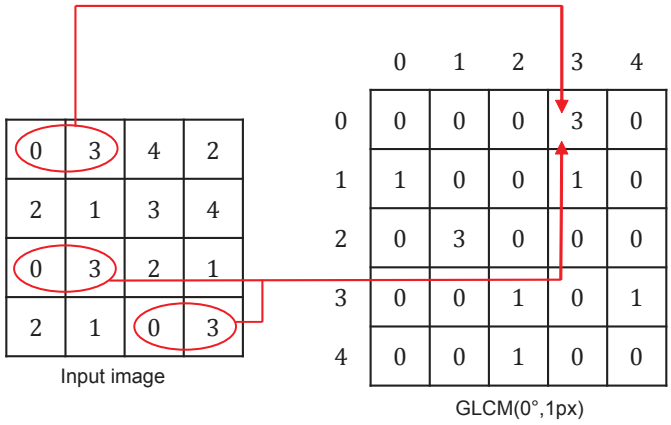

FIGURE 1. Example of calculation of the GLC Matrix using a position operator of one horizontally pixel from an input image with five grey levels.

Figure 1 shows on the right the calculated GLC Matrix using the position operator of one horizontally pixel. In the GLC Matrix, element (1,4) contains the value 3 because there is three instances in the input image where two horizontally adjacent pixels have the values 0 and 3, respectively. Similarly, element (4,5) contains the value 1 because there is only one instance where two horizontally adjacent pixels have the values 3 and 4. The Grey Level co-occurrence Matrix contains an important amount of data. However, it cannot be used directly. Hence, fourteen parameters have been defined by Haralick [7] so that textural features can be characterized using the GLC Matrix. The most widely adopted parameters are the contrast, correlation, energy and homogeneity. Once the GLC Matrix is calculated, it is normalized, so that the sum of its components (called $p(i, j)$) is equal to 1. Then, the four statistical parameters (contrast, correlation, energy and homogeneity) are extracted.

Image Processing

In order to distinctly segment warp and weft yarns, a threshold using the most pertinent parameter is performed on 3D orthogonal non-crimp woven fabric. This should result in a concentration of information inside the yarn sections and as few as possible disruptive pixels outside of them. Homogeneity is the best parameter for extracting yarn sections (Fig. 2d). Contrast (Fig. 2a) and energy (Fig. 2c) separate the yarns as well, however, there is less information inside the sections when compared with the homogeneity method.

Moreover, applying a smoothing filter on the parameter can facilitate the threshold. By using a 3D Gaussian filter or a 3D Median filter, it is possible to homogenize the image information: the yarn sections appear more complete. Furthermore, the yarns' cross sections are often not full enough. Additional mathematical morphology operations (closing, convex hull) are needed to attain acceptable yarn cross sections and to achieve segmented volume (Fig. 3).

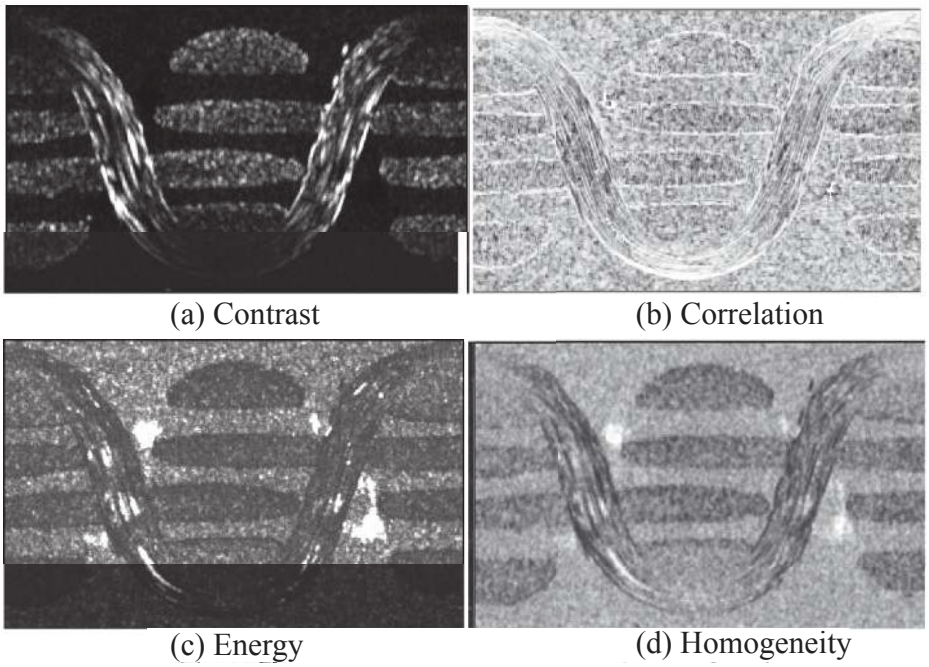

FIGURE 2. GLCM's statistical parameters applied to 3D reinforcement.

FIGURE 3. 3D orthogonal non-crimp segmented volume.

MESH GENERATION

In meso-scale textile composite modelling, the yarn is considered as a 3D domain. Meshes of the yarn have been generated with hexahedral elements and tetrahedral elements. Nevertheless, neither of these element shapes is completely satisfactory. The hexahedral elements are numerically more efficient and they are well adapted to describe the yarn in the fibre direction [6,8,9]. However, it is difficult to mesh the transverse section of the yarn in a suitable manner. Most of the composite yarns have a lenticular shape and, therefore, both extremities are difficult to mesh. On the other hand, the tetrahedral elements can mesh any volume and they efficiently describe the transverse section of the yarn. However, a mesh based on tetrahedrons needs a large number of elements to be sufficiently accurate. In the present

work, a prismatic element mesh generator is used [10]. The section is meshed with the triangle edge of the prisms and the quadrangle edges are in the fibre's direction.

CONSTITUTIVE LAW OF THE YARN

A hyperelastic constitutive law is used to describe the mechanical behaviour of fibre bundles of woven composite reinforcements at finite strain [6].

Hyperelastic Constitutive Equation

The potential energy can be written as a function of the right Cauchy-Green strain tensor $\underline{\underline{C}}$:

$$w = w\left(\underline{\underline{C}}\right) \quad with \quad \underline{\underline{C}} = \underline{\underline{F}}^T . \underline{\underline{F}} \tag{1}$$

The symmetry group of a transversely isotropic material is characterised, in the initial configuration, by a unit vector $\underline{M}$ which represents the preferred direction. This allows the definition of a structural tensor $\underline{\underline{M}} = \underline{M} \otimes \underline{M}$. Then, the strain energy potential becomes:

$$w = w\left(I_1, I_2, I_3, I_4, I_5\right) \tag{2}$$

where I_1, I_2, I_3 are the invariants of $\underline{\underline{C}}$ defined by:

$$I_1 = Tr\left(\underline{\underline{C}}\right) \qquad I_2 = \frac{1}{2}\left(Tr\left(\underline{\underline{C}}\right)^2 - Tr\left(\underline{\underline{C}}^2\right)\right) \qquad I_3 = Det\left(\underline{\underline{C}}\right) \tag{3}$$

and where I_4 and I_5 are mixed invariants defined from the structural tensor $\underline{\underline{M}}$

$$I_4 = \underline{\underline{C}} : \underline{\underline{M}} \quad I_5 = \underline{\underline{C}}^2 : \underline{\underline{M}} \tag{4}$$

The contribution of each deformation mode is considered as independent from the others; the second PiolaKirchhoff stress tensor is then defined as:

$$\underline{\underline{S}} = 2\frac{\partial w}{\partial \underline{\underline{C}}} = \left(\frac{\partial w}{\partial I_1}\frac{\partial I_1}{\partial \underline{\underline{C}}} + \frac{\partial w}{\partial I_2}\frac{\partial I_2}{\partial \underline{\underline{C}}} + \frac{\partial w}{\partial I_3}\frac{\partial I_3}{\partial \underline{\underline{C}}} + \frac{\partial w}{\partial I_4}\frac{\partial I_4}{\partial \underline{\underline{C}}} + \frac{\partial w}{\partial I_5}\frac{\partial I_5}{\partial \underline{\underline{C}}}\right) \tag{5}$$

Physically Based Invariants

The behaviour law is based on the physics of the tow deformation [6]. Four deformation modes can be identified: elongation in the fibre direction, compaction in the transverse section of the yarn, distortion (shear) in the transverse section and shear along the fibre direction. The last mode (longitudinal shear) mainly controls the bending rigidity of the yarn. It is a compound of two equivalent deformation modes corresponding to the two directions of shear. The following set of invariants, corresponding to these four deformation modes, is defined in function of the classical invariants I_1 to I_5 defined above:

$$I_{elong} = \frac{1}{2}\ln\left(I_4\right), \quad I_{comp} = \frac{1}{4}\ln\left(\frac{I_3}{I_4}\right), \quad I_{dist} = \frac{1}{2}\ln\left(\frac{I_1 I_4 - I_5}{2\sqrt{I_3 I_4}} + \sqrt{\left(\frac{I_1 I_4 - I_5}{2\sqrt{I_3 I_4}}\right)^2 - 1}\right), \quad I_{sh} = \sqrt{\frac{I_5}{I_4^2} - 1} \tag{6}$$

These invariants are used to define the strain energy functions associated to each deformation mode:

$$w\left(\underline{\underline{C}}\right) = w\left(I_{elong}, I_{comp}, I_{dist}, I_{sh}\right) \tag{7}$$

Finally, the whole constitutive equation is the summation of all contributions discussed above:

$$\underline{\underline{S}} = 2\left(\frac{\partial w_{elong}}{\partial I_{elong}}\frac{\partial I_{elong}}{\partial \underline{\underline{C}}} + \frac{\partial w_{comp}}{\partial I_{comp}}\frac{\partial I_{comp}}{\partial \underline{\underline{C}}} + \frac{\partial w_{dist}}{\partial I_{dist}}\frac{\partial I_{dist}}{\partial \underline{\underline{C}}} + \frac{\partial w_{sh}}{\partial I_{sh}}\frac{\partial I_{sh}}{\partial \underline{\underline{C}}}\right) = \underline{\underline{S}}_{elong} + \underline{\underline{S}}_{comp} + \underline{\underline{S}}_{dist} + \underline{\underline{S}}_{sh} \quad (8)$$

The constitutive law depends on eight parameters: four corresponding to longitudinal elongation, two to yarn compaction, one to yarn distortion and one to longitudinal shear. This constitutive equation has been implemented as a user material subroutine VUMAT in the ABAQUS/Explicit finite element code.

MESO-SCALE F.E SIMULATIONS

Meso-scale F.E. simulations of transverse compaction are performed on the 3D orthogonal non-crimp woven fabric. The material parameters are displayed in [10]. The initial section of the yarn,S_0, is determined by mesoscale observations of the fabric, using X-ray tomography for instance. The three other parameters are identified with a tensile test on a single yarn. Since the yarn may have been damaged during weaving, this test must be performed on a yarn extracted from the fabric rather than before weaving. The others parameters come from [6]. Figure 4 shows geometries obtained by tomography and simulation of the 3D reinforcement submitted to a transverse compaction.

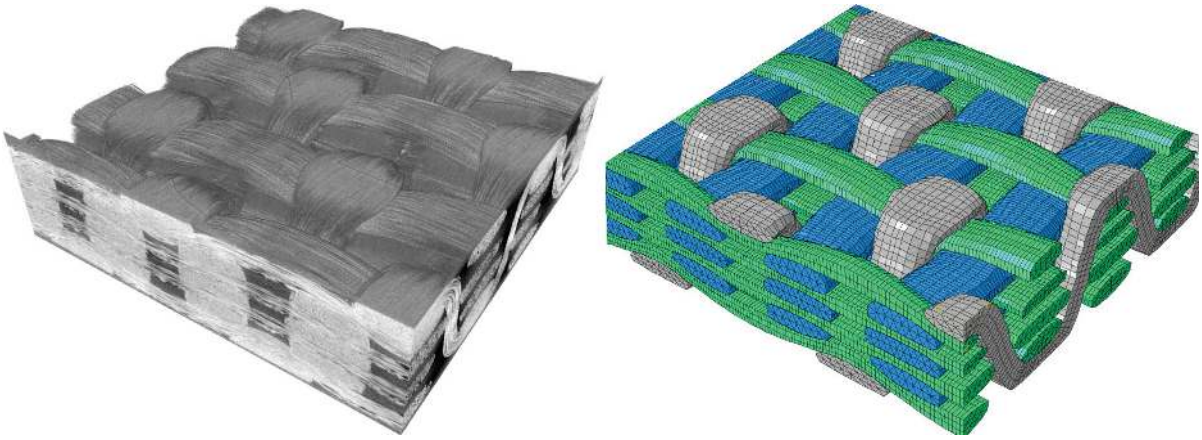

FIGURE 4. Comparison between the compacted tomography and the 3D orthogonal non-crimp woven simulation.

The reinforcement was crushed to 22 % of its original length between two plexiglass plates linked by four screws. The crushing of the binder yarn obtained in the simulation is consistent with tomography. The computed deformed geometry is in agreement with the geometry obtained from tomography. Figure 5 shows the comparison between the experimental and computed compaction loads (loads on the compression machine). These loads are coherent.

CONCLUSION

X-ray tomography is well adapted to the development of 3D textile composite meso-FE models directly from reinforcement specimens. The complexity of their geometry and of the yarn interlacing can be taken into account with μCT images. A segmentation method based on image texture has been explored to separate the warp, weft and binder yarns in the μCT images. This approach is better adapted to the study than a structure tensor approach commonly used for 2D fabrics because the yarns are oriented in all directions of space. The yarns are meshed by prism finite elements. This shape is well suited to fibrous yarn geometry. The triangle edges mesh the transverse section of the tows. Meso-F.E. analyses have been performed using a hyperelastic model developed previously for fibre bundles. This constitutive law is well adapted to these simulations. The comparisons between experimental trials and the computed internal deformed geometry have shown coherent results. This method must now be applied in other cases in order to check its robustness. Moreover, the meso-FE is used in the computation of 3D reinforcement permeability. The composite reinforcement is compacted and/or sheared before the resin injection phase of the R.T.M process. The internal geometry after compaction or shearing can be used to perform flow analyses and determine the permeability properties.

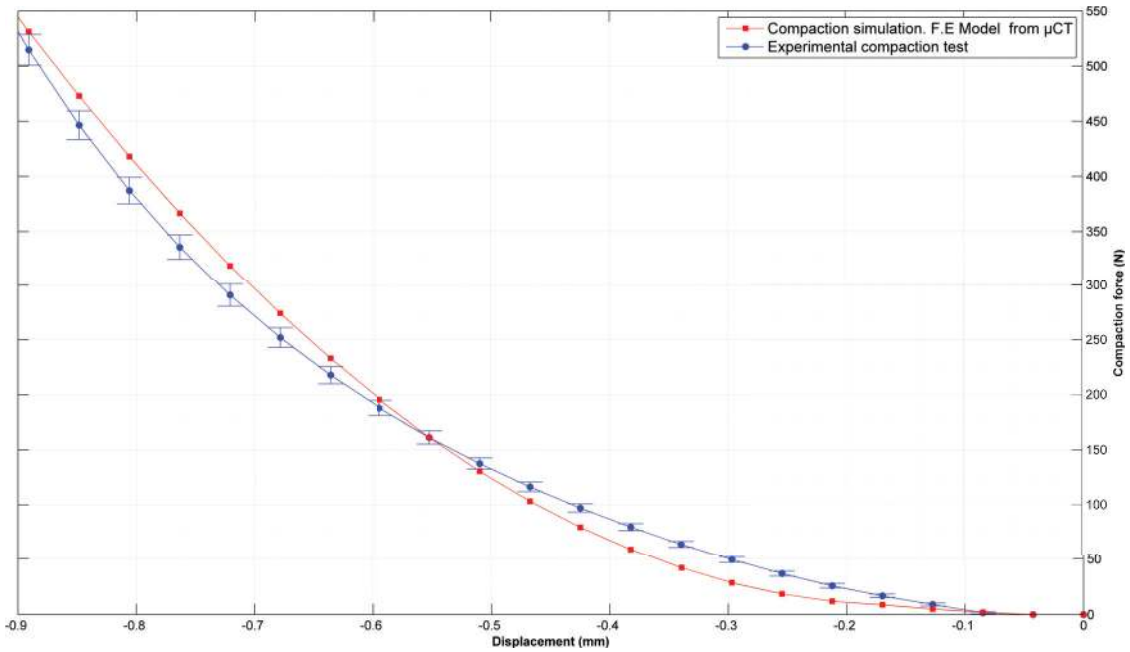

FIGURE 5. Comparison between simulated and tomographied 3D orthogonal non-crimp woven compacted to 22%.

ACKNOWLEDGMENTS

The authors thank the support of INSIS-CNRS for this study.

REFERENCES

[1] A. Long and L. Brown, in *Composite reinforcements for optimum performance*, edited by Boisse (Woodhead Publishing, 2011), pp. 239–264.

[2] S. V. Lomov, in *Composite reinforcements for optimum performance*, edited by Boisse (Woodhead Publishing, 2011), pp. 200–238.

[3] J. Baruchel, J. Buffiere, E. Maire, P. Merle, and G. Peix, *X-Ray Tomography in Material Science*, edited by J. Baruchel, J. Buffiere, E. Maire, P. Merle, and G. Peix (Hermes Science, 2000).

[4] N. Naouar, E. Vidal-Salle, J. Schneider, E. Maire, and P. Boisse, Composite Structures **116**, 165–176 (2014).

[5] M. Barburski, I. Straumit, X. Zhang, M. Wevers, and S. V. Lomov, Composites Part A: Applied Science and Manufacturing **73**, 45–54 (2015).

[6] A. Charmetant, Vidal-Salle, and P. Boisse, Composites Science and Technology **71**, 1623–1631 (2011).

[7] R. Haralick, K. Shanmugam, and I. Dinstein, IEEE Transactions on Systems, Man and Cybernetics - TSMC **3**, 610–621 (1973).

[8] A. Wendling, G. Hivet, E. Vidal-Salle, and P. Boisse, Finite Elements in Analysis and Design **90**, 93–105 (2014).

[9] E. Obert, F. Daghia, P. Ladeveze, and L. Ballere, Composite Structures **117**, 212–221 (2014).

[10] N. Naouar, E. Vidal-Salle, J. Schneider, E. Maire, and P. Boisse, Composite Structures **132**, 1094–1104 (2015).